Geomechanics and Engineering, *Vol. 17, No. 3 (2019) 227-236*
DOI: https://doi.org/10.12989/gae.2019.17.3.227

Discretization technique for stability analysis of complex slopes

Chaoqun Hou[1a], Tingting Zhang[1b], Zhibin Sun*[1], Daniel Dias[1,2c] and Jianfei Li[1d]

[1]School of Automotive and Transportation Engineering, Hefei University of Technology, No. 193, Tunxi Road, China
[2]Laboratory 3SR, Grenoble Alpes University, CNRS UMR5521, France

(Received November 30, 2018, Revised December 28, 2018, Accepted January 30, 2019)

Abstract. In practice, the natural slopes are frequently with soils of spatial properties and irregular features. The traditional limit analysis method meets an inherent difficulty to deal with the stability problem for such slopes due to the normal condition in the associated flow rule. To overcome the problem, a novel technique based on the upper bound limit analysis, which is called the discretization technique, is employed for the stability evaluation of complex slopes. In this paper, the discretization mechanism for complex slopes was presented, and the safety factors of several examples were calculated. The good agreement between the discretization-based and previous results shows the accuracy of the proposed mechanism, proving that it can be an alternative and reliable approach for complex slope stability analysis.

Keywords: stability analysis; upper bound limit analysis; complex slopes; safety factor; slip surface

1. Introduction

The stability of soil slope has drawn a wide attention across the geotechnical community. To solve the problem, numerous methods have been proposed, which can be classified into the following three types.

(1) Limit equilibrium (LE).

LE is the traditional method to assess the slope stability, which consists of the Bishop method, Janbu method, and so on. With LE, a slip surface is assumed and the soil mass above the surface can be divided into a series of slices. Global static equilibrium along various surfaces will be checked. By the introduction of the notion of the safety factor, the most dangerous surface permits to be sought.

LE is attractive and popular due to its simple calculation procedure and the ability to gain effective results. However, there lies a limitation that it does not consider the stress-strain relation of soils (Chen 2003). And some statical assumptions, which are necessary to avoid indeterminate condition will lead to the imprecise results. Besides, results from such analyses are sometimes ambiguous due to the different assumptions (Michalowski 1998). Thus it is difficult to assess the accuracy of such solutions by LE (Leshchinsky 2015).

(2) Numerical simulation technique.

With the development of the computer, the numerical simulation methods have been widely used. Such methods supply better and comprehensive information, such as stresses, movements, progressive failure, and so on, which are not possible by LE (Sloan 2013, Aksoy *et al*. 2016, Keawsawasvong and Ukritchon 2016, Bhattacharya and Roy 2016, Babanouri and Sarfarazi 2018).

However, the time in modeling and computing is much larger than that in LE, and the convergence is not an easy process, too. For some complicated cases, the results are very sensitive to the size of the elements, the tolerance of the analysis and the number of iteration (Cheng *et al*. 2007), which enforces the need for caution in applying this approach in the assessment of complex slopes.

(3) Limit analysis (LA).

LA has been developed in a more rigorous way than LE with respecting the plasticity theory (Chen 1975). And LA can be simpler since it does not require special constitutive laws and the complex material parameters associated with the application of the numerical analyses.

With LA, there are two approaches to bracket the limit solutions of structures: the static approach and the kinematic approach. The former one, which gives a lower bound of the limit solution, needs to determine a statically admissible stress field. And the latter one, which gives an upper bound of the limit solution, needs to search a kinematical admissible velocity field (Chen and Liu 1990, Yang and Li 2018, Zhang *et al*. 2018, Xu and Yang 2019). The static approach is seldom used since the admissible stress fields are uneasy to construct. Conversely, it is simpler to define a kinematical admissible velocity field, which makes the kinematical approach more widespread.

In the application of the kinematical approach, the failure surface is commonly described by a logarithmic spiral curve, which is in accordance with the associated flow rule (Michalowski 1995, Kumar 2000, Aminpour *et al*.

*Corresponding author, Assistant Professor
E-mail: sunzb@hfut.edu.cn
[a]Associate Professor
E-mail: houcq@hfut.edu.cn
[b]M.Sc. Student
E-mail: 1109053704@qq.com
[c]Professor
E-mail: daniel.dias@univ-grenoble-alpes.fr
[d]M.Sc. Student
E-mail: 1562228662@qq.com

http://www.techno-press.org/?journal=gae&subpage=7
ISSN: 2005-307X (Print), 2092-6219 (Online)

2017, Li and Yang 2018a, Li and Yang 2019a). However, due to the tedious calculation process, it is inconvenient to apply such curve in the cases with non-homogeneous properties (Kumar 2006, Nian *et al*. 2008).

To solve the problem, Mollon *et al*. (2013) proposed an innovative kinematic approach based on a 'point-to-point' technique. This discretization technique was then successfully applied in slope engineering by Qin and Chian (2017), and the results were proved to be in good agreement with previous achievements.

To further validate the discretization technique, the present study focuses on its implementation in complex slopes (layered slopes or benched slopes). In addition, the authors try to illustrate and clarify some aspects of the wide applicability of the limit analysis based on the discretization technique.

This paper was organized as follows. A brief introduction of the discretization mechanism and the calculation of the work rates are firstly presented. Then the calculation of the safety factor, which is incorporated into a numerical procedure, is introduced. This is followed by the presentation of the extended discretization mechanisms for different types of complex slopes. Finally, several cases of complex slopes are discussed and conducted.

2. Collapse mechanism analysis

2.1 Collapse mechanism generation

In this paper, the discretization mechanism is utilized for the stability estimations of complex slopes. This section aims at presenting the main principle for the generation of this mechanism. It is detailed as follows.

The proposed discretization mechanism is illustrated in Fig. 1. The slope height H and slope angle β are the necessary parameters to describe the slope geometry. A coordinate system is established with the slope toe C being the origin.

The mechanism is assumed to rotate rigidly around the rotational center O with the angular velocity ω. And the entire mechanism is fully defined by two parameters r_0 and θ_0, where r_0 is the length of OC and θ_0 is the angle between x axis direction and line OC.

In this mechanism, the slip surface AC is discretized by a series of straight segments P_iP_{i+1}. It is worth mentioning that each segment P_iP_{i+1} should make an angle φ_i with the velocity vector $\vec{v}_i$ in order to enforce the associated flow rule. Thus the generation process aims to define all the discretization point P_i.

A 'point to point' technique was used herein to determine the discretization points along the slip surface, which means that each point is derived from the previous one. The generation process starts at point C, namely the first point P_0 on the slip surface, and terminates to the last point P_n on the slope crest.

In order to make all the discretization points distributed evenly, the angle between OP_i and OP_{i+1} is considered as a constant $\delta\theta$. The value of $\delta\theta$ also influences the accuracy of the failure mechanism. A smaller value of $\delta\theta$ makes more precise result, but the computation process is also more

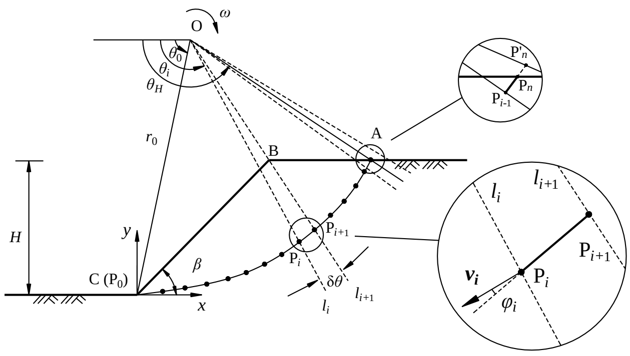

Fig. 1 Discrete failure mechanism of slopes

time-consuming. Herein $\delta\theta$ is set to be equal to 0.1°, which was recommended as a great combination of accuracy and time cost (Sun *et al*. 2017).

In summary, the mathematical formulation from point P_i to point P_{i+1} can be described as

$$\begin{cases} x_{i+1} = x_i + \dfrac{\sqrt{(x_i - x_O)^2 + (y_i - y_O)^2} \times \sin\delta\theta}{\sin(\pi/2 + \varphi - \delta\theta)} \times \cos(\theta_i - \pi/2 + \varphi) \\ y_{i+1} = y_i + \dfrac{\sqrt{(x_i - x_O)^2 + (y_i - y_O)^2} \times \sin\delta\theta}{\sin(\pi/2 + \varphi - \delta\theta)} \times \sin(\theta_i - \pi/2 + \varphi) \end{cases} \tag{1}$$

where x_i and y_i are the abscissa and ordinate of the point P_i, x_{i+1} and y_{i+1} are the abscissa and ordinate of the point P_{i+1}, x_O and y_O are the abscissa and ordinate of the point O, it can be defined as

$$\begin{cases} x_O = r_0 \cos\theta_0 \\ y_O = r_0 \sin\theta_0 \end{cases} \tag{2}$$

The generation terminates when the generated points reach the slope crest. If the ordinate of the last discrete point is greater than the slope height H, i.e., $y_i > H$, the last generated point is replaced by the junction between the last discrete segment and the slope crest using linear interpolation method.

2.2 Calculation of the work rates

In upper bound theorem, the stability conditions were determined by the work equation, which states that the external work rate W is no more than the energy dissipation D (Yang and Li 2018, Li and Yang 2018b, Li and Yang 2019b). In the present study, the external work rate is provided by the weight of the collapsed block ABCA, and the internal energy dissipation only occurs along the slip surface AC due to the rigid block assumption.

The gravity work rate can be achieved by the summation of the work rate per discretization block BP_iP_{i+1}. As shown in Fig. 2, the gravity work rate of block BP_iP_{i+1} can be written as

$$W_i = \vec{G}_i \cdot \vec{v}_{Gi} = \gamma\omega S_i R_{Gi} \cos\theta_{Gi} \tag{3}$$

where γ is the unit weight, S_i is the triangle BP_iP_{i+1} area, R_{Gi} is the distance between the barycenter P_{Gi} of triangle BP_iP_{i+1} and the rotating center O, θ_{Gi} is the angle between OP_{Gi} and the horizontal direction. Thus the gravity work rate of the

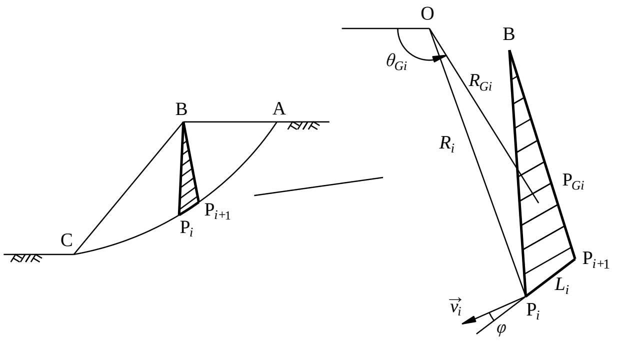

Fig. 2 Analysis of the discrete block BP_iP_{i+1}

failure mechanism can be defined

$$W=-\gamma\omega\sum S_i R_{Gi}\cos\theta_{Gi} \tag{4}$$

Similarly, the energy dissipation per infinitesimal unit is added along the velocity discontinuity and permits to obtain

$$D=\omega\sum c_i L_i R_i \cos\varphi_i \tag{5}$$

where c_i and φ_i are the cohesion and internal friction angle of point P_i, L_i is the length of an elementary segment P_iP_{i+1}, R_i is the distance between point O and point P_i.

2.3 Computation flow of the safety factor

The calculating examples illustrated in the present study assess the slope stability using the safety factor F_s, which is also recommended in many design codes. F_s is commonly determined by the shear strength reduction method, which can make the slope achieve a limit state by reducing given shear strength parameters. The reduced parameters c_f and φ_f can be defined as (Griffths and Lane 1999, Chen *et al.* 2003, Nian *et al.* 2008)

$$\begin{cases} c_f = c/F_s \\ \varphi_f = \arctan(\tan\varphi/F_s) \end{cases} \tag{6}$$

Normally, the nonlinear safety factor equation can be given when the reduced strength parameters are introduced into constraints imposed by equating the external work rate to the energy dissipation. However, with discretization technique, such function is unavailable because the work rates of the discretization mechanism are calculated by summation. Thus, a novel numerical procedure is proposed to determine the value of F_s after the mechanism generation. It can be expressed as

Step 1: Set the search range of parameters. The search ranges of θ_0, r_0 and F_s are $[\beta,\pi]$, $[0.5H, 10H]$ and $[F_{s1}, F_{s2}]$ respectively.

Step 2: Assign the Strength Reduction Factor (SRF) to $\mathrm{SRF}=(F_{s1}+F_{s2})/2$, and reduce the strength parameters c and φ by SRF. Then introduce the modified parameters c_f and φ_f into the equation which the external work rate equals the energy dissipation. Search the least value of the absolute difference between W and D: $\min|W-D|$ where the two parameters were performed.

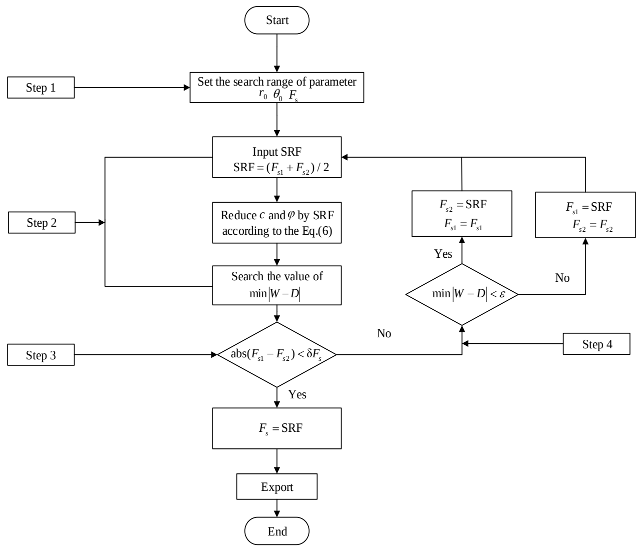

Fig. 3 Flow chart of the optimization

Step 3: Evaluate the value of δF_s and the absolute difference between F_{s2} and F_{s1}. If $\mathrm{abs}(F_{s1}-F_{s2})<\delta F_s$, the searching process will end, and the safety factor F_s is equal to SRF. Otherwise, the procedure enters step 4. δF_s is a prescribed parameter which determines the accuracy of the solutions, namely 0.01 in this study.

Step 4: Estimate the value of $\min|W-D|$, if $\min|W-D|=0$, SRF is an upper bound solution of the safety factors and then F_{s2}=SRF. Otherwise F_{s1}=SRF.

Then, the procedure enters step 2 and the next iteration. It is employed iteratively in order to determine the least upper bound solution of F_s.

In the search program of step 2, the inherent error makes the value of $\min|W-D|$ always greater than zero even in a velocity admissible mechanism, while $\min|W-D|$ is supposed to be equal to zero theoretically. Hence a threshold value ε is introduced to perform the evaluation in step 4. To our experience, it can be set to $5\mathrm{kN}\cdot\mathrm{m}^3$ for $\delta\theta=0.1^\circ$.

The detailed computation flow chart of safety factor is described in Fig. 3.

3. Stability analyses for complex slopes

3.1 Non-homogeneous slopes cases

The soil exhibits non-homogeneity in its properties due to the geological and environmental effects (Pan and Dias 2016, Khezri *et al.* 2016, Xu *et al.* 2018). The non-homogeneity of soils has two common forms:

(1) The strength parameters are distributed linearly with depth as shown in Fig. 4(a) (Nian *et al.* 2008);

(2) The strength parameters vary in different soil layers as shown in Fig. 4(b) (Kumar 2006).

The discretization technique has been proven to be valid in the first case (Sun *et al.* 2017), therefore the validation of

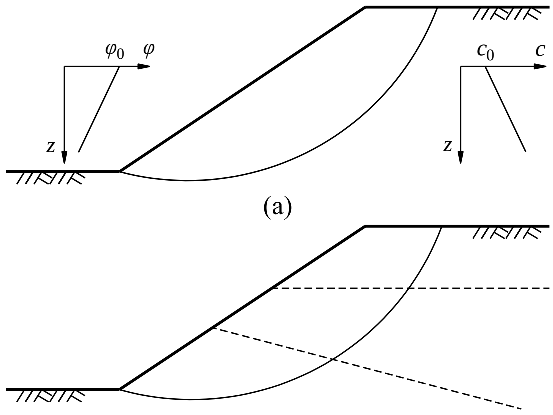

Fig. 4 Two types of nonhomogeneous slopes

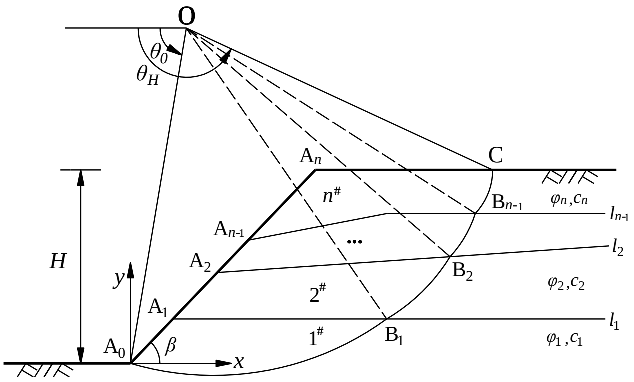

Fig. 5 Discrete failure mechanism of the layered slope

the second case is focused on herein. The presentation of the mechanism generation and the work rates computation are shown as follows.

A slope with various soil layers is illustrated in Fig. 5. There exist n soil layers, which are separated by layer line l_j, where $j \in [1, n]$. The values of the internal friction angle φ_j and the cohesion c_j of each layer are different. And it is further assumed that the value of the unit weight is constant.

The normality rule enforces the slip surface making an angle φ with the velocity vector. Thus the slip surface generation is conducted layer by layer in this layered slope. More concretely, in soil layer $1^{\#}$, the generation starts at point A_0, proceeds with the constraints that P_iP_{i+1} makes an angle φ_1 with v_i, and terminates when the point P_{i+1} above line l_1. Then the interpolation method, which is mentioned in the above section, is carried out to gain the end point (point B_1) of the slip surface in layer$1^{\#}$. Afterward, the surface generation in layer $2^{\#}$ begins from the point B_1 and so on. The construction of the entire slip surface terminates when the endpoint C is achieved.

The work rate of gravity is related to the soil density, of which distribution is uniform herein. Therefore the calculation of the gravity work rate can be performed according to Eq. (4). Differently, the dissipation work rate along the slip surface is involved with the value of φ_j and c_j. Hence the energy dissipation of entire slip surface is provided by the summation of that in each layer. The expression is

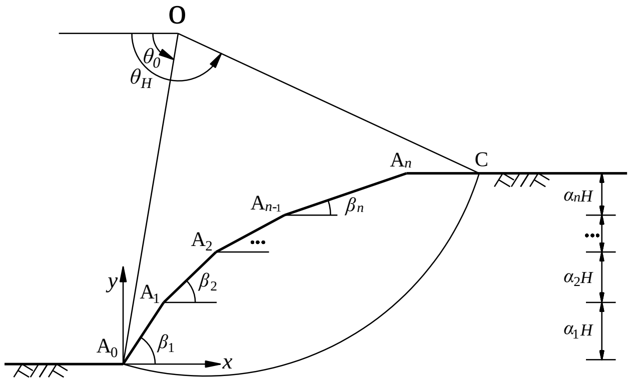

Fig. 6 Discrete failure mechanism of the multi-stage convex slope

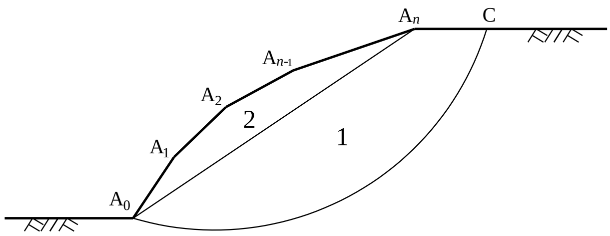

Fig. 7 Block division of convex slopes

$$D = \omega \sum_{j=1}^{n} \sum_{i=1}^{i_j} L_i R_i c_i \cos \varphi_i \tag{7}$$

where i_j is the amount of discrete segments for each layer.

3.2 Multi-stage slopes cases

Two typical forms of slopes with irregular geometries are defined in the present study, i.e., the convex slope in Fig. 6 and the benched slope in Fig. 8 (Gao *et al.* 2013, Xiao *et al.* 2015). For simplicity, the soil is considered to be homogenous in this section.

A convex slope with n stages is described in Fig. 6. The slope height is H and the proportion of each stage is α_j, where $j \in [1, n]$. The slope surface of each stage is inclined at an angle β_j with the horizontal direction. A_0C is the slip surface.

The generation process of slip surface is identical with that in a homogeneous slope. However, due to the complex geometries, the calculation method of work rates is diverse from that of the simple slope.

As shown in Fig. 7, the sliding soil mass is divided into two blocks, namely $A_0A_nCA_0$ and $A_0A_1A_2A_{n-1}A_nA_0$. The first block can be treated as a simple slope as shown in Fig. 1, while the second block is a polygon bounded with n+1 straight lines. Thus the total gravity work rate of the convex slope W is contributed by the two items. More details can be found in Appendix 1. Moreover, the energy dissipation is easily arrived by the Eq. (5).

Another frequent type of irregular slopes, the benched slope is more popular in practical engineering. As demonstrated in Fig. 8, the height of each stage is α_jH and the slope angle of each stage is β_j, where $j \in [1, n]$. The

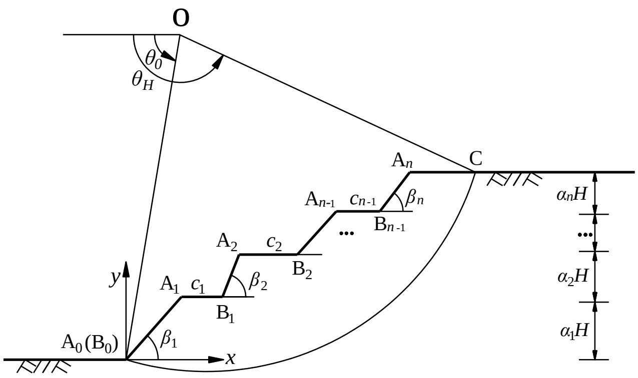

Fig. 8 Discrete failure mechanism of the multi-stage benched slope

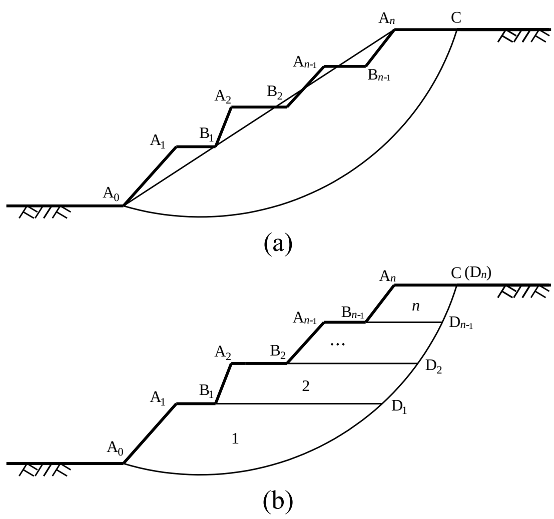

Fig. 9 The block division of the multi-stage benched slope

length of each bench $A_{j-1}B_{j-1}$ is denoted by c_{j-1}. A_0C is the slip surface.

As shown in Fig. 9(a), the gravity work rate of convex slopes cannot be achieved by the way of connecting point A_0 and point A_n. Thus the block division approach will be carried out as depicted in Fig. 9(b), the platform line A_jB_j is extended to the slip surface A_0C with the point of D_j. The collapse block is divided into n blocks by the line A_jD_j. Thus the gravity work rate of the entire block W can be considered as

$$W = \sum_{j=1}^{n} W_j \tag{8}$$

where W_j is the gravity work rate of the block j.

The gravity work rate of the block 1 can be solved easily by treating this block as a simple slope. However, note that the shape of the other blocks is different from the block 1. For these blocks, the calculation process of W_j needs to be modified. More details can be found in Appendix 2. The energy dissipation can also be given by Eq. (5).

4. Discussions of numerical examples

In this section, the results of the several cases using

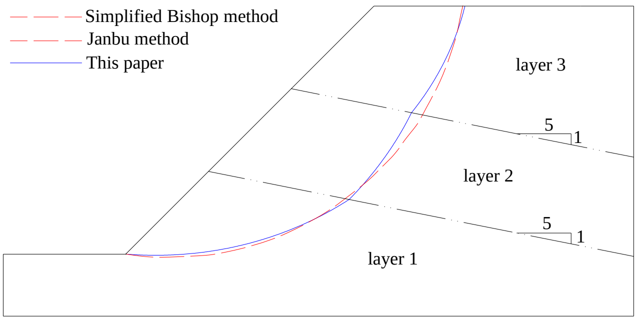

Fig. 10 Comparison of the critical slip surface for example 1

Table 1 Soil properties for example 1

Layer	φ[°]	c[kPa]	γ[kN/m^3]
1	15	20.4	18.82
2	30	30.4	18.82
3	15	20.4	18.82

Table 2 Comparison of the safety factor for example 1

Number	Calculation methods	F_s
1	Bishop method	1.308
2	Janbu method	1.325
3	This paper	1.269

discretization method are compared with the previous results, in order to validate the effectiveness of the discretization mechanism in the analysis of the complex slopes.

4.1 Layered slopes

Example1 : Inclined layered slope

The geometry of the layered slope with 3 inclined layers is shown in Fig. 10 and the soil properties are given in Table 1. It is noted that the shear strength parameters of layer 1 and layer 3 are entirely the same while layer 2 has higher values of friction angle and cohesion. The height of the slope is 12m, and the slope surface inclines at 45° with the horizontal line. Both of hierarchical lines are determined by tanβ=1/5, where β is the angle between the inclined layers and the horizontal direction.

As listed in Table 2, the safety factor of the present method is 1.269, which is lower than the value obtained by the Bishop and Janbu methods. The differences with respect to the Bishop method and the Janbu method are 3.07% and 4.41% respectively.

Fig. 10 presents the comparisons of slip surfaces with these methods. The three sliding surfaces are consistent in the first layer, while in the second and third layers, the one by the discretization method is different from the slip surfaces specified by other two methods.

The reason for the discrepancy can be explained as follows. In the discretization mechanism, the angle between slip surface and the horizontal direction is equal to $\theta_i + \varphi_i - \pi/2$. The friction angle of layer 2 is higher than

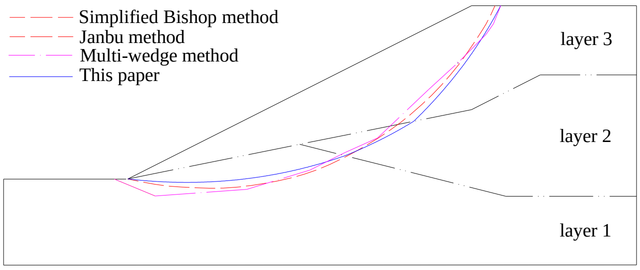

Fig. 11 Comparison of the critical slip surface for example 2

Table 3 Soil properties for example 2

Layer	φ[°]	c[kPa]	γ[kN/m^3]
1	20	7.2	19.5
2	23	5.3	19.5
3	38	0	19.5

Table 4 Comparison of the safety factor for example 2

Number	Calculation methods	F_s
1	Bishop method	1.405
	Spencer method	1.375
	GLE method	1.374
2	Multi-wedge method	1.378-1.393
3	This paper	1.381

the ones of layers 1 and 3. Thus, the slip surface becomes steeper in layer 2 and slows down with the decrease of the friction angle from layer 2 to layer 3.

The slip surfaces which were obtained by the Bishop and Janbu methods are circular, while the one provided by the discretization method appears less ‘regular’. It can be noted that the discretization-based slip surface is consistent with the variation of the friction angle, which indicates that the discretization mechanism is more realistic and suitable for non-homogeneous slope analysis.

Example 2：Irregular layered slope

Fig. 11 presents the trail profiles of an irregular layered slope with complex characteristics (Slide Verification manual 2003). The geometrical data consists of H=10 m and tanα=1/2, where α is the slope angle. There are three layers in this slope. For each layer, the unit weight remains constant while the strength parameters are different (Table 3). Table 4 and Fig. 11 present the comparisons of the safety factors and the critical slip surfaces, as given by the discretization mechanism, the multi-wedge method (Anthony 1999) and LE (Slide Verification manual 2003).

As seen in Table 4, the discretization-based safety factor is almost the same as the existing solutions, except for that by the Bishop method. This consistency demonstrates that the discretization mechanism is efficient. Besides, it can be observed in Fig. 11 that the failure surface agrees well with these ones obtained by the other methods. However, there still lie some nuances.

The slip surface by the discretization method is not a single line but is composed of serval non-standard curves. Such slip surface is consistent with the variations of shear strength parameters. Note that the friction angle difference between the layer 2 and layer 3 is relatively large (15°), the slip surface specified by present method has an obvious transition of the failure surface from layer 2 to layer 3.

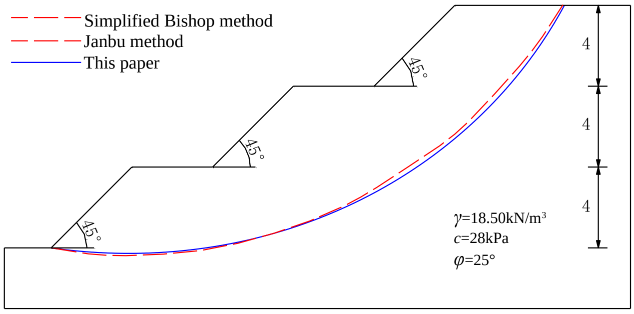

Fig. 12 Comparison of the critical slip surface for example 3

Table 5 Comparison of the safety factor for example 3

Number	Calculation methods	F_s
1	Bishop method	2.212
2	Janbu method	2.220
3	This paper	2.203

The present method is more advanced for layered slope stability analysis due to the competence of not only providing a kinematical admissible solution but also making the slip surface consistent with the friction angle variation.

4.2 Multi-stage slopes

This section focuses on the possible improvement of the discretization mechanism for multi-stage slopes. The comparisons of two different examples will be offered.

Example 3：Three-stage benched slope

Fig. 12 considers a homogeneous benched slope with three stages. The height and width of each bench are 4m, and the slope angle of each stage is 45°. The cohesion and friction angle are 28 kPa and 25° respectively, and the unit weight is kept at 18.50 kN/m^3. The discretization results were compared with those existing methods, which are shown in Table 5 and Fig. 12.

Safety factors in Table 5 show the results based on different methods are close. The present method gave a safety factor of 2.203. This value is slightly lower than these ones given by the Bishop and Janbu methods, which were estimated equal to 2.212 and 2.220 respectively. It indicates that the present method permits to calculate the safety factor of multi-stage benched slopes. Besides, as shown in Fig. 12, the discretization-based slip surface agrees well with those of LE. This case proved that the discretization method can give accurate solutions for a multi-stage slope.

Example 4：Complex slope

An irregular three-stage slope is shown in Fig. 13 according to Xiao *et al*. (2015). The height of the slope is 15 m, the slope angles for the lower part and the upper part are 45° respectively, while the middle part angle α is defined by tanα=1/2. The soil properties are the unit weight γ=20 kN/m^3, the cohesion c=10 kPa, and the friction angle φ=20°.

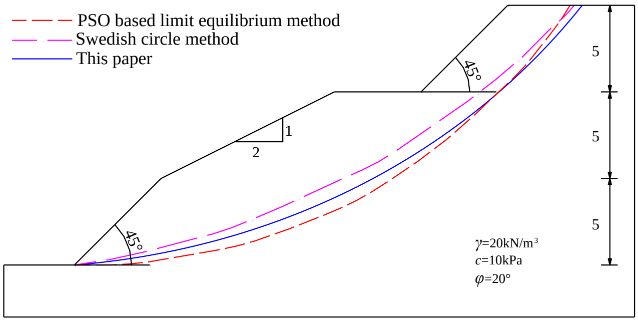

Fig. 13 Comparison of the global critical slip surface for example 4

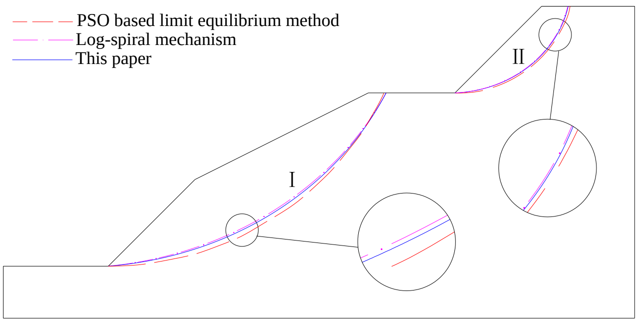

Fig. 14 Comparison of the local critical slip surfaces for example 4

Table 6 Comparison of the safety factor for example 4

Case	Calculation methods	F_s
Global slip surface	PSO based LE	1.118
	Swedish circle method	1.145
	This paper	1.154
Local slip surface of case I	PSO based LE	1.076
	Log-spiral mechanism	1.106
	This paper	1.109
Local slip surface of case II	PSO based LE	1.156
	Log-spiral mechanism	1.272
	This paper	1.272

Slope failure does not always occur progressively. Sometimes the soil reaches an ultimate state in a different location initially and then extends to other places (Cheng *et al.* 2007, Xiao 2015). Namely, except for one defined critical slip surface, the slope could also slide along other surfaces. Thus the complex slope geometry could result in multiple slip surfaces.

As shown in Figs. 13 and 14, a global critical slip surface and two potential local slip surfaces can be identified. From Fig. 13, it can be seen clearly that although there is not a perfect agreement in the description of the critical slip surfaces, the same trend is obtained. Additionally, the present slip surface is located between the ones by the PSO and the Swedish circle methods, which demonstrates that the present method is reasonable. Two potential slip surfaces were analyzed as presented at location I and location II in Fig. 14. Both local slip surfaces are similar to those obtained from the other methods, with being more nearer to those by the log-spiral mechanism. The consistency further validates the accuracy of the method presented in this study.

The comparisons of the calculated safety factors are presented in Table 6. For local slip surfaces, the difference of F_s can be up to 10.03% between the discretization method and the PSO method. However, the log-spiral mechanism and the discretization method give similar results. For the case of global slip failure, the value of F_s achieved by three methods are also close.

The above two multi-stage slope examples indicate that the discretization mechanism is rational in multi-stage slopes.

4.3 Natural slopes

This section analyzed a natural slope landslide of Tianshenqiao Hydro-power Project which is located on the right bank of the Nanpanjiang River, Guangxi Province in China (Chen and Shao 1988, Donald and Chen 1997, Malkawi *et al*. 2001).

The geometrical and geological profile is shown in Fig. 15. There are 7 layers and the geotechnical parameters used in the slope stability analysis are listed in Table 7.

The comparisons of the optimized results (safety factor) are presented in Table 8. Chen and Shao (1988)

Table 7 Soil properties for the natural slope

Layer	φ[°]	c[kPa]	γ[kN/m³]
1	21.79	19.6	18.13
2	21.79	19.6	18.13
3	24.79	0.0	18.13
4	20.79	29.38	18.13
5	10.18	34.29	17.75
6	24.2	0	18.62
7	45.0	39.3	23.54

Table 8 Comparison of the safety factor

Number	Calculation methods	F_s
1	Spencer's Method	0.863
2	EMU	0.882
3	Monte Carlo	0.712
4	This paper	0.793

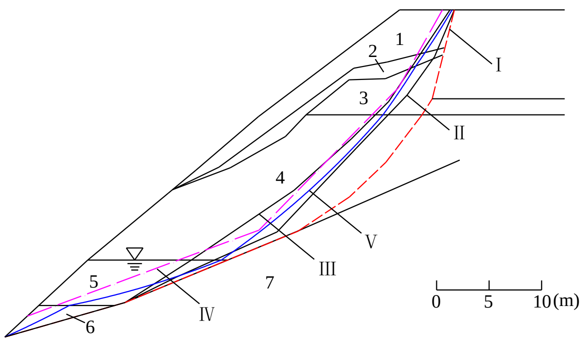

Fig. 15 Comparison of the failure surfaces for natural slope: Failure surface I. Actual, II. Spencer's Method (Chen and Shao, 1988), III. EMU (Donald and Chen, 1997), IV. SAS-MCT (Malkawi *et al.* 2001) and V. Present discretization method

analyzed this slope with Spencer's Method and obtained the safety factor as 0.863. It was later discussed by Donald and Chen (1997) using the computer program Energy Method Upper bound (EMU) and the optimized result is 0.882. And the safety factor obtained by Malkawi *et al*. (2001) using Stability Analysis of Slopes and Monte Carlo Techniques (SAS-MCT) is equal to 0.712. Basing on the discretization mechanism, this slope was analyzed in this paper and the factor of safety is 0.793, which is in the range of 0.712 to 0.882.

Besides, the actual failure surface and critical slip surfaces optimized by various methods are also displayed in Fig. 15. It can be seen that the present slip surface have the same trend with the actual one and the surfaces obtained by the other methods, which passes all the layers except the layer 7. And it is located between the slip surfaces optimized by the SAS-MCT and the Spencer's Method. Moreover, the friction angle of the layer 5 is 10.18°, which is significantly lower than the one of layer 6 (24.2°). So there is a distinct transition on the surface from layer 6 to layer 5 due to the consideration of the strength parameters in the generation of the slope failure surface.

Both of the comparisons of safety factors and the failure surfaces between this paper and the existed researches demonstrate the effectiveness and practicability of the present discretization method in the analysis of natural slope stability.

5. Conclusions

This paper aims at validating the discretization mechanism in the complex slopes, which contains the multi-layer slopes with varying strength parameters, the multi-stage slopes with complex geometries and natural slopes.

The generation of discretization mechanisms and the establishment of work rates equations for complex slopes were described. The computational flow chart of safety factor was also detailed. Then through several complex examples with the existing results, the validation was carried out. The present methods can be demonstrated by the good agreements in both safety factors and slip surfaces.

In addition, the slip surfaces of layered slope are not single lines but are composed of several non-standard curves, which are more realistic from the point of the view of plastic theory. The discretization mechanism has the potential to be an effective tool in analyzing the stability of complex geotechnical structures in scenarios of varied strata and the complicated geometries. Since it not only can assure the kinematically admissible solution, but also can avoid the tedious mechanism generation process.

The discretization method opens a wide application of kinematical analysis for slopes with non-homogeneity and complex geometries. And it can also be used in other geotechnical structures, such as foundations and retaining walls.

Acknowledgements

The research described in this paper was financially supported by the Natural Science Foundation National Natural Science Foundation (51408180).

References

Aksoy, C.O., Uyar, G.G. and Ozcelik, Y. (2016), "Comparison of Hoek-Brown and Mohr-Coulomb failure criterion for deep open coal mine slope stability", *Struct. Eng. Mech.*, **60**(5), 809-828

Aminpour, M.M., Maleki, M. and Ghanbari, A. (2017), "Investigation of the effect of surcharge on behavior of soil slopes", *Geomech. Eng.*, **13**(4), 653-669.

Anthony, T.G. (1999), "Genetic algorithm search for critical slip surface in multiple-wedge stability analysis", *Can. Geotech. J.*, **36**(2), 382-391.

Babanouri, N. and Sarfarazi, V. (2018), "Numerical analysis of a complex slope instability: Pseudo-wedge failure", *Geomech. Eng.*, **15**(1), 669-676.

Bhattacharya, P. and Roy, A. (2016), "Improvement in uplift capacity of horizontal circular anchor plate in undrained clay by granular column", *Geomech. Eng.*, **10**(5), 617-633.

Chen, J., Yin, J. and Lee, C.F. (2003), "Upper bound limit analysis of slope stability using rigid finite elements and nonlinear programming", *Can. Geotech. J.*, **40**(6), 742-752.

Chen, W.F. (1975), *Limit Analysis and Soil Plasticity*, Elsevier Scientific Publishing Company, New York, U.S.A.

Chen, W.F. and Liu, X.L. (1990), *Limit Analysis in Soil Mechanics*, Elsevier Scientific Publishing Company, New York, U.S.A.

Chen, Z.Y. (2003), *Stability Analysis of Earth Slopes: Principle, Method and Program*, China Water Conservancy and Hydropower press, Beijing, China.

Chen, Z.Y. and Shao, C.M. (1988), "Evaluation of minimum factor of safety in slope stability analysis", *Can. Geotech. J.*, **25**(4), 735-748.

Cheng, Y.M., Lansivaara, T. and Wei, W.B. (2007), "Two-dimensional slope stability analysis by limit equilibrium and strength reduction methods", *Comput. Geotech.*, **34**(3), 137-150.

Donald, I.B. and Chen, Z.Y. (1997), "Slope stability analysis by the upper bound approach: Fundamentals and methods", *Can. Geotech. J.*, **34**(6), 853-862.

Gao, L.S., Zhao, L.H., Tang, G.P. and Luo, W. (2013), "Upper bound limit analysis of stability on inhomogeneity and anisotropy two-stage slope", *Elec. J. Geotech. Eng.*, **18**, 3581-3604.

Griffiths, D.V. and Lane, P.A. (1999), "Slope stability analysis by finite elements", *Géotechnique*, **49**(7), 653-654.

Keawsawasvong, S. and Ukritchon, B. (2016), "Ultimate lateral capacity of two dimensional plane strain rectangular pile in clay", *Geomech. Eng.*, **11**(2), 235-251.

Khezri, N., Mohamad, H. and Fatahi, B. (2016), "Stability assessment of tunnel face in a layered soil using upper bound theorem of limit analysis", *Geomech. Eng.*, **11**(4), 471-492.

Kumar, J. (2000), "Slope stability calculations using limit analysis", *Proceedings of the Geo-Denver 2000- Educational Issues in Geotechnical Engineering*, Denver, Colorado, U.S.A., August.

Kumar, J. and Samui, P. (2006), "Stability determination for layered soil slopes using the upper bound limit analysis", *Geotech. Geol. Eng.*, **24**(6), 1803-1819.

Leshchinsky, B. (2015), "Limit equilibrium and limit analysis: Comparison of benchmark slope stability problems", *J. Geotech. Geoenviron. Eng.*, **141**(10), 04015043.

Li, Y.X. and Yang, X.L. (2018a), "Three-dimensional seismic displacement analysis of rock slopes based on Hoek-Brown failure criterion", *KSCE J. Civ. Eng.*, **22**(11), 4334-4344.

Li, Z.W. and Yang, X.L. (2018b), "Active earth pressure for soils with tension cracks under steady unsaturated flow conditions", *Can. Geotech. J.*, **55**(12), 1850-1859.

Li, Y.X. and Yang, X.L. (2019a), "Soil-slope stability considering effect of soil-strength nonlinearity", *Int. J. Geomech.*, **19**(3), 04018201.

Li, Z.W. and Yang, X.L. (2019b), "Kinematical analysis of active earth pressure considering tension crack, pore-water pressure and soil nonlinearity", *KSCE J. Civ. Eng.*, **23**(1), 56-62.

Malkawi, A.I.H., Hassan, W.F. and Sarma, S.K. (2001), "Global search method for locating general slip surface using Monte Carlo techniques", *J. Geotech. Geoenviron. Eng.*, **127**(8), 688-698.

Michalowski, R.L. (1995), "Slope stability analysis a kinematical approach", *Géotechnique*, **45**(2), 283-293.

Michalowski, R.L. (1998), "Limit analysis in stability calculations of reinforced soil structures", *Geotext. Geomembranes*, **16**(6), 311-331.

Mollon, G., Dias, D. and Soubra, A.H. (2013), "Continuous velocity fields for collapse and blowout of a pressurized tunnel face in purely cohesive soil", *Int. J. Numer. Anal. Meth. Geomech.*, **37**(13), 2061-2083.

Nian, T.K., Chen, G.Q., Luan, M.T., Yang, Q. and Zheng, D.F. (2008), "Limit analysis of the stability of slopes reinforced with piles against landslide in nonhomogeneous and anisotropic soils", *Can. Geotech. J.*, **45**(8), 1092-1103.

Pan, Q.J. and Dias, D. (2016), "Face stability analysis for a shield-driven tunnel in anisotropic and nonhomogeneous soils by the kinematical approach", *Int. J. Geomech.*, **16**(3), 1-11.

Qin, C.B. and Chian, S.C. (2017), "Kinematic analysis of seismic slope stability with a discretization technique and pseudo-dynamic approach: a new perspective", *Géotechnique*, **68**(6), 492-503.

Rocscience Inc. (2003), *Slide Verification Manual*, Rocscience Inc., Toronto, Canada.

Sloan, S.W. (2013), "Geotechnical stability analysis", *Géotechnique*, **63**(7), 531-572.

Sun, Z.B., Pan, Q.J., Yang, X.L., Hou, C.Q. and Shang, M.T. (2017), "Discrete mechanism for the upper bound analysis of nonhomogeneous slope", *Chin. J. Rock Mech. Eng.*, **36**(7), 1680-1688.

Xiao, S., Li, K., Ding, X. and Liu, T. (2015), "Numerical computation of homogeneous slope stability", *Comput. Intell. Neurosci.*, 12.

Xu, J.S. and Yang, X.L. (2019), "Seismic stability of 3D soil slope reinforced by geosynthetic with nonlinear failure criterion", *Soil Dyn. Earthq. Eng.*, **118**, 86-97.

Xu, J.S., Li, Y.X. and Yang, X.L. (2018), "Seismic and static 3D stability of two-stage slope considering joined influences of nonlinearity and dilatancy", *KSCE J. Civ. Eng.*, **22**(10), 3827-3836.

Yang, X.L. and Li, Z.W. (2018), "Comparison of factors of safety using a 3D failure mechanism with kinematic approach", *Int. J. Geomech.*, **18**(9), 04018107.

Zhang, J.H., Wang, W.J., Zhang, D.B., Zhang, B. and Meng, F. (2018), "Safe range of retaining pressure for three-dimensional face of pressurized tunnels based on limit analysis and reliability method", *KSCE J. Civ. Eng.*, **22**(11), 4645-4656.

JS

Appendix 1

As shown in Fig. 7, the external work rate for the multi-stage convex slope can be written as

$$W = W_1 + W_2 \tag{9}$$

(i) W_1 refers to the rate of the gravity work of the block $A_0A_nCA_0$. It can be calculated by the given method of the simple slope, i.e., Eq. (4).

(ii) W_2 denotes the gravity work rate of the block $A_0A_1A_2A_{n-1}A_nA_0$, namely the polygons with n+1 lines, and it can be written as

$$W_2 = -\gamma\omega S_2 R_{G2} \cos\theta_{G2} \tag{10}$$

where R_{G2} is the distance between the barycenter P_G of the block $A_0A_1A_2A_{n-1}A_nA_0$ and rotation center O, and the coordinates of the barycenter P_G can be defined as

$$\begin{cases} x_{R_{G2}} = \dfrac{1}{n+1}\sum\limits_{i=1}^{n+1} x_i \\ y_{R_{G2}} = \dfrac{1}{n+1}\sum\limits_{i=1}^{n+1} y_i \end{cases} \tag{11}$$

where x_i and y_i is the abscissa and ordinate of the point A_j. S_2 is the area of the polygon. The block $A_0A_1A_2A_{n-1}A_nA_0$ herein can be divided into $n-1$ triangles $A_0A_jA_{j+1}$. Adding the triangle's area together permits to obtain the value of S_2.

Appendix 2

As shown in Fig. 16, line A_jB_{j-1} is extended to the slip surface at point E_{j-1}. Then block $A_jE_{j-1}D_jA_j$ and block $B_{j-1}E_{j-1}D_{j-1}B_{j-1}$ are yielded. Both of them can be treated as the simple slope. Thus the gravity work rate of block j can be obtained by subtracting the block $B_{j-1}E_{j-1}D_{j-1}B_{j-1}$ from the block $A_jE_{j-1}D_jA_j$. For the sake of convenience, the gravity work rates of the of blocks $A_jE_{j-1}D_jA_j$ and $B_{j-1}E_{j-1}D_{j-1}B_{j-1}$ are abbreviated as A_j and B_{j-1}, respectively. The work rate of block j permits to be obtained as

$$W_2 = W_{A_2} - W_{B_1} \tag{12}$$

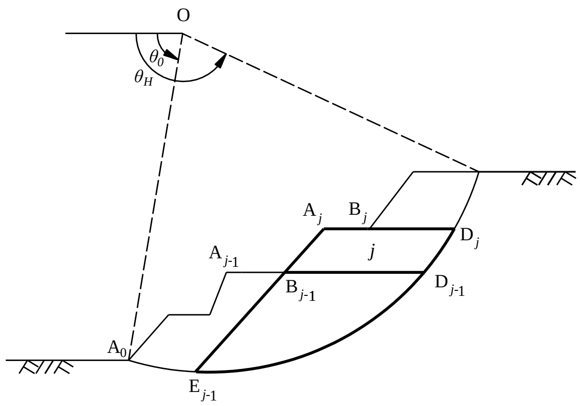

Fig. 16 Principle of the gravity work rate calculation for block j